Journal of Geochemical Exploration 184 (2018) 28–39

Contents lists available at ScienceDirect

Journal of Geochemical Exploration

journal homepage: www.elsevier.com/locate/gexplo

Fluid and melt inclusion study on mineralized and barren porphyries, Jinshajiang-Red River alkali-rich intrusive belt, and significance to metallogenesis

Die Wang[a,b], Xianwu Bi[a,*], Huanzhang Lu[a,c], Ruizhong Hu[a], Xinsong Wang[a], Leiluo Xu[a]

[a] State Key Laboratory of Ore Deposits Geochemistry, Institute of Geochemistry, Chinese Academy of Sciences, Guiyang 550002, China
[b] Faculty of Land and Resources Engineering, Kunming University of Science and Technology, Kunming 650031, China
[c] University of Quebec, Chicoutimi, Quebec G7H 2B1, Canada

ARTICLE INFO

Keywords:
Fluid/melt inclusion
Phenocryst mineral
Porphyry Cu (Au, Mo) deposit
Jinshajiang–Red River alkali-rich intrusive belt

ABSTRACT

Alkali-rich Cu (Au, Mo) deposits are of increasing economic significance and are an attractive exploration target. They include some of the world's highest grade and largest porphyry related gold resources as well as some of the largest gold accumulations in epithermal settings. The Jinshajiang–Red River alkali-rich intrusive belt, with many porphyry Cu (Au, Mo) deposits, is a representative magmatic belt associated with mineralization. The Jinshajiang–Red River alkali-rich intrusive belt contains several Cu (Au, Mo) mineralized alkali-rich porphyry rocks including the Yulong quartz monzonite porphyry, the Machangqing granite porphyry, the Tongchang quartz syenite porphyry, and the Beiya quartz syenite porphyry. Additionally, there are also some barren alkali-rich porphyry rocks in the belt, such as the Yanshuiqing quartz syenite porphyry. Fluid inclusion petrography and microthermometry on those porphyry rocks are carried out in detail. The results show that the fluid inclusion assemblages in ore-bearing and barren porphyries are distinct: inclusions from barren porphyry are dominated by primary melt inclusions, and contain rare or no fluid inclusions, whereas inclusions from ore-bearing porphyries are dominated by fluid inclusions, and contain rare melt inclusions. Furthermore, halite, sylvite, calcite daughter minerals and an opaque phase in fluid inclusions from ore-bearing rocks are common, but rare in fluid inclusions from barren rocks. The results suggests that the evolution of ore forming fluids especially the halite, sylvite, calcite and opaque daughter minerals bearing fluid inclusions of quartz phenocrysts could be used to judge the degree of metasomatism and mineralization of a porphyry system.

1. Introduction

Fluid and melt inclusions are now widely used in various fields of geology, especially in the study of metallogenesis. The small droplets of melt/fluid trapped in minerals preserve information on the composition and evolutionary conditions of hydrothermal and magmatic systems, and therefore are the most direct evidence of physical and chemical conditions of the environment during magmatic crystallization (e.g., Sobolev and Danyushevsky, 1994; Sobolev, 1996; Audetat et al., 1998, 2008; Halter et al., 2005; Ulrich et al., 1999; Wilkinson et al., 2009).

Porphyry deposits are the most important sources of copper, aurum and molybdenum, accounting for approximately 75% of the world's copper resource, and 95% of molybdenum reserves (Sillitoe, 2010). Porphyry rocks mainly occur in two types of tectonic environments: (1) the island-arc and continental–arc settings, and (2) the intra-continental tectonic setting (Hou et al., 2003; Cooke et al., 2005; Sillitoe, 2010; Wang et al., 2012, 2015). Alkali-rich Cu (Au, Mo) deposits are of increasing economic significance and are an attractive exploration target. They include some of the world's highest grade and largest porphyry related gold resources as well as some of the largest gold accumulations in epithermal settings.

Over the past 20 years, abundant studies have been conducted on the formation and evolutionary processes of alkali-rich-magmatic systems, associated with Cu (Au, Mo) mineralization in the island-arc and continental-arc settings, indicating that mineralization related magmas with high oxygen fugacity and enrichment in H_2O and other volatile components, were produced by oceanic-slab subduction (Bi et al., 2002; Richards, 2003; Cooke et al., 2005; Liang et al., 2009; Sillitoe, 2010). However, the studies on intra-continental alkali-rich magmatic systems are very limited, which restricts the understanding of ore-forming mechanisms of alkali-rich magma systems in intra-continental tectonic setting.

* Corresponding author at: State Key Laboratory of Ore Deposit Geochemistry, Institute of Geochemistry, Chinese Academy of Sciences, China.
E-mail address: bixianwu@vip.gyig.ac.cn (X. Bi).

http://dx.doi.org/10.1016/j.gexplo.2017.09.016
Received 11 November 2014; Received in revised form 28 September 2017; Accepted 28 September 2017
Available online 04 October 2017
0375-6742/

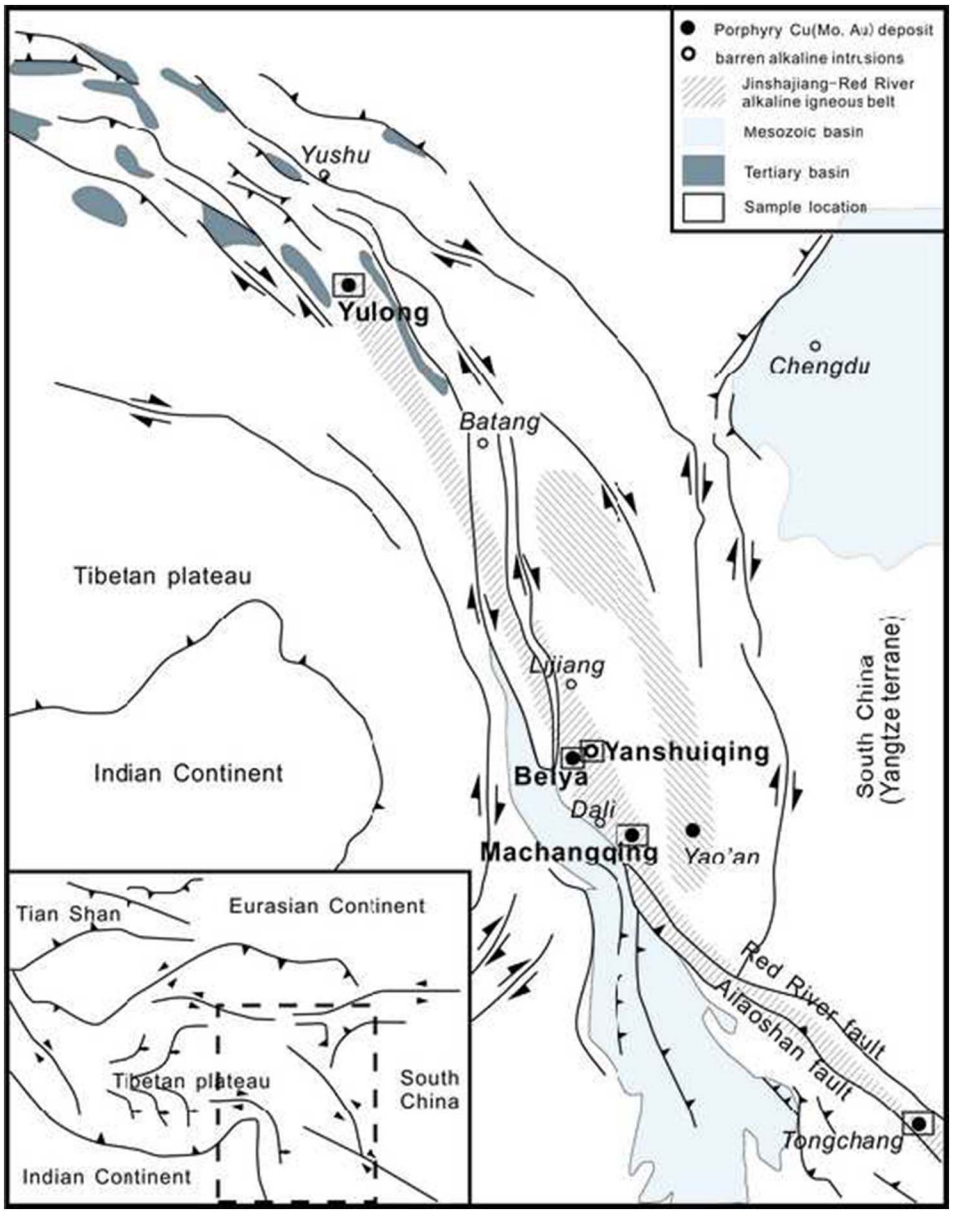

Fig. 1. Simplified geological map showing the Cenozoic tectonic framework and the distribution of porphyry Cu (Mo, Au) deposits in the Jinshajiang–Red River alkali-rich intrusive belt.
(modified from Hou et al., 2006)

The Jinshajiang–Red River alkali-rich intrusive belt, with many porphyry Cu (Au, Mo) deposits, is a representative magmatic belt associated with mineralization in a continental tectonic setting (Bi et al., 2002, 2004; Hou et al., 2003, 2007; Hu et al., 1998, 2004; Zhao et al., 2002). Cu (Au, Mo)-mineralized alkaline intrusions are distributed along the belt, and most of them were formed in the Cenozoic in similar tectonic setting, but their mineralization potential differs among the different intrusions (Bi et al., 2005, 2009; Chung et al., 1998; Jiang et al., 2006; Liang et al., 2006, 2007; Wang et al., 2001; Wang et al., 2004; Xu et al., 2006; Xu, 2011; Xu et al., 2012). In this study, fluid and melt inclusion petrography and microthermometry studies were carried out in detail to assess the difference between barren and mineralized porphyry intrusions.

2. Regional geologic setting and deposits geology

The Jinshajiang–Red River alkali-rich intrusive belt is developed along the eastern Indo-Asian collision zone in western China (Fig. 1). This magmatic belt is over 2000 km long and 50–80 km wide. In recent years numerous Cu (Au, Mo) deposits, which are spatially related to and contemporaneous with those alkaline intrusions, have been discovered in the area (Bi et al., 2002, 2004; Hou et al., 2003, 2007; Hu et al., 1998, 2004; Zhao et al., 2002). Cu (Au, Mo)-mineralized alkaline intrusions, such as the Yulong quartz monzonite porphyry, the Machangqing granite porphyry, the Tongchang quartz syenite porphyries, the Beiya quartz syenite porphyry. Some barren alkaline intrusions also occur in the belt, such as the Yanshuiqing quartz syenite porphyry, are distributed along the belt (Fig. 1). The age dating of those intrusions indicates that the ages of magmatism ranges from 45 Ma to 33 Ma, and they are felsic with $K_2O + Na_2O$ (usually > 8 wt%), show a potassic or high-K calc-alkaline affinity like arc alkaline rocks related to Cu- and Au-deposits in circum-Pacific regions (Chung et al., 1998; Liang et al., 2006, 2007; Wang et al., 2001; Wang et al., 2004; Jiang et al., 2006; Xu et al., 2006; Xu, 2011; Xu et al., 2012). These intrusions formed in a rift or crustal extension tectonic setting (Bi et al., 2005; Chung et al., 1997, 1998; Gu et al., 2003; Hou et al., 2003; Jiang et al., 2006; Tu, 1989; Turner et al., 1996; Wang et al., 2001; Zhang et al., 1987; Zhang and Xie, 1997).

2.1. The Yulong porphyry Cu (Au, Mo) deposit

The Yulong porphyry Cu (Au, Mo) ore belt is > 400 km long and 15–30 km wide and is one of the largest porphyry Cu (Au, Mo) deposits in China, that occurs on the eastern margin of the Tibetan plateau. Six porphyry Cu (Au, Mo) deposits including Narigongma (reserves of 0.25 Mt. Cu at 0.33% and 0.675 Mt. Mo at 0.079%), Yulong (reserves of 6.5 Mt. Cu at 0.38% and 0.15 Mt. Mo at 0.04%), Malasongduo (reserve of 1.0 Mt. Cu at 0.44%), Duoxiasongduo (reserve of 0.50 Mt. Cu at 0.38%), Zhanaga (reserve of 0.30 Mt. Cu at 0.36%) and Mangzong (reserve of 0.25 Mt. Cu at 0.34%), and > 20 Cu-Mo-Au porphyry prospects have been identified in this belt, with a total resource of Cu and Mo exceeding 10 Mt (Hou et al., 2003).

The rock type of mineralized porphyry of the Yulong deposit is mainly quartz monzonite porphyry with a zircon U-Pb age of 43.2 ± 0.25 Ma (Xu, 2011) emplaced into late Triassic limestone. The surface area of the mineralized porphyry is approximately 0.64 km^2. The mineralogy consists of plagioclase, K-feldspar, amphibole, biotite, quartz, and accessory minerals include magnetite, titanite, apatite and zircon. Early alteration, associated with porphyry Cu - Au - Mo mineralization, produced concentric alteration zones ranging from an inner K-silicate zone through a quartz–sericite zone to an outer propylitic zone (Hou et al., 2006). Sixteen samples from the Yulong quartz monzonite porphyry are chosen for the study, and all of the samples are underwent K-silicate and phyllicalteration.

2.2. The Machangqing porphyry Cu (Mo, Au) deposit

The Machangqing deposit is a representative porphyry Cu (Mo, Au) deposit in the middle of the Jinshajiang–Red River alkali-rich intrusive belt. About 200,000 t of Cu was estimated, with the average ore grade being 0.5% (Bi et al., 2009). The rock type of mineralized porphyry is mainly granite porphyry and quartz monzonite porphyry both with a zircon U-Pb age of 35.0 ± 0.2 Ma (Liang et al., 2006) emplaced into the lower Ordovician micro clastic rocks and Devonian limestones. Both types of the porphyry are formed by K-feldspar, plagioclase, amphibole, mica, quartz, and accessory minerals include magnetite, titanite, apatite and zircon.

Porphyry-type and skarn-type ores constitute two major mineralization styles in the Machangqing copper deposit. The Machangqing intrusive body exhibits strong hydrothermal alteration that forms more or less concentric zones extending outward from the inner part of the intrusion, including a silicification zone, a K-silicate zone, a propylitic zone and an argillic zone. The silicification zone is characterized by veins and stockworks of quartz. The K-silicate zone is characterized by pervasive alteration of plagioclase to orthoclase, and hornblende and primary biotite to secondary biotite. The alteration was accompanied by disseminated and veinlet-type Cu-sulfide mineralization. Propylitic alteration is weak but pervasive forming a wide halo in the country rocks and overprinting into other alteration zones. The main assemblage consists of epidote, chlorite, albite and calcite. Weak argillic alteration is characterized by the replacement of biotite and feldspar by clay minerals. Fifteen samples of Machangqing quartz monzonite porphyry were chosen for the study; all of the samples had undergone weak K-silicate and phyllicalteration.

2.3. The Tongchang porphyry Cu (Mo, Au) deposit

The Tongchang Cu (Mo, Au) deposit lies in the southern segment of the Jinshajiang–Red River alkali-rich intrusive belt and has relatively small-scale mineralization. Three stages of magmatism occurred in the Tongchang ore field, including the early stage of fine-grained syenites, the middle stage of quartz syenite porphyries, and the late stage of syenite porphyries, diabases and diabase gabbros. The Cu (Mo, Au) mineralization occurs primarily within and around the middle stage of quartz syenite porphyries with a zircon U–Pb age of 35.79 ± 0.22 Ma (Xu et al., 2012) and was emplaced into the middle Silurian limy dolomite. The molybdenite Re-Os age of ca. 34 Ma (Xu et al., 2012) for the Tongchang deposit indicates that the Cu (Mo, Au) mineralization was closely related to the quartz syenite porphyries. The quartz syenite porphyry is composed of K-feldspar, amphibole, biotite, quartz, and accessory minerals including magnetite, titanite, apatite and zircon. The ores occur as Cu (Mo, Au) veinlets within the stock that underwent K-silicate, phyllic alteration, and as Cu (Mo, Au) skarns developed between the stock and limestone. Eighteen samples of Tongchang quartz syenite porphyry are chosen for the study, and the samples are underwent a weak K-silicate and phyllicalteration.

2.4. The Beiya porphyry Au-polymetallic deposit

The Beiya Au-polymetallic deposit is located in the middle of the Jinshajiang–Red River alkali-rich intrusive belt and has relatively large scales of mineralization, which was estimated at > 100 t Au when mining Cu, Ag, Fe, Pb and Zn at the same time. The rock type of mineralized porphyry is mainly quartz syenite porphyry with a biotite ^{39}Ar-^{40}Ar age of 25.5–32.5 Ma (Xu et al., 2006).Wall rocks in the Beiya area are Late Permian basalt, Lower Triassic sandstone, Middle Triassic limestone, and Tertiary lacustrine and quaternary sedimentary rocks. The Middle Triassic limestone is the 550 m-thick Beiya group that is one of the main host rocks of ore and is characterized by intensive karst development. The ores occur as polymetallic veinlets within the stock that underwent K-silicate and phyllic alteration, and as polymetallic skarns developed between the intrusion and limestone. Associated with porphyry Au-polymetallic mineralization, concentric alteration zones were produced ranging from an inner K-silicate zone through a phyllic zone and a chloritization zone to an outer skarns ore zone. Fourteen samples of Beiya quartz syenite porphyry were chosen for the study, all of the samples had undergone K-silicate and phyllicalteration.

2.5. The Yanshuiqing barren igneous rocks

The Yanshuiqing barren alkaline igneous rocks occur in the middle part of the Jinshajiang–Red River alkali-rich intrusive belt. The Yanshuiqing barren alkaline igneous rocks located in the Heqing county of Yunnan close to the Beiya Au-polymetallic deposit. The alkaline igneous rocks are quartz syenite porphyry with the zircon U-Pb age is 37.10 ± 0.75 Ma (Xu, 2011). The Yanshuiqing quartz syenite porphyry is mainly formed by K-feldspar, plagioclase, quartz and amphibole. The Yanshuiqing quartz syenite porphyry is fresh and 13 samples were chosen for the study.

3. Inclusion petrography and microthermometry

3.1. Inclusions classification

Doubly polished plates (approximately 200 μm thick) of 76 samples from the above-mentioned mineralized and barren igneous rocks were prepared for the study. Fresh samples were chosen as far as possible, however, all of the samples from Cu (Au, Mo)-mineralized porphyry underwent K-silicate and phyllic alteration, only samples from barren porphyry are fresher.

Sections were examined in both petrography and thermometry to determine and analyze the fluid and melt inclusion in quartz phenocryst and vein quartz of the intrusions and four types of inclusions were recognized (Fig. 2).

I-type: Silicate melt inclusions (SMI for short in this issue, see

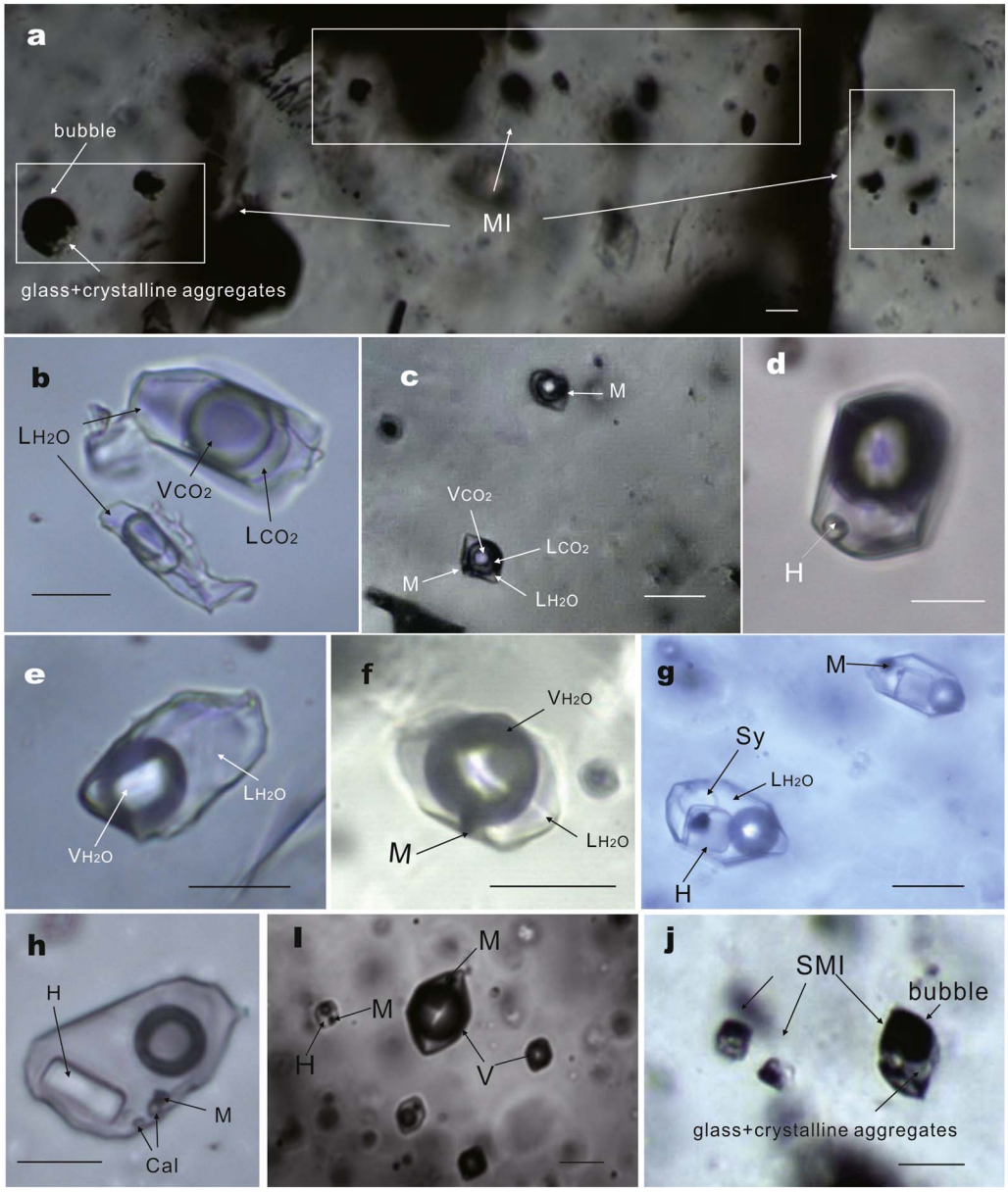

Fig. 2. Photomicrographs of four types of inclusions. The scale is 10 μm. M-metal daughter mineral; H-halite; Cal-calcite; SMI-silicate melt inclusion. a. I-type crystallized SMI in quartz along the crystal growth zone with round shapes (from Yanshuiqing); b. III_a-type CO_2-rich fluid inclusions (V_{CO2} + L_{CO2} + L_{H2O}) (from Beiya); c. III_b-type, CO_2-rich fluid inclusions with metal daughter mineral (V_{CO2} + L_{CO2} + L_{H2O} + opaque daughter-mineral) (from Tongchang); d. IV_a-type, halite daughter mineral-bearing fluid inclusions with negative crystal shape (from Yulong);e. II-type, two-phase aqueous inclusions (from Yanshuiqing); f. IV_b type, opaque daughter mineral-bearing inclusions (from Yulong); g. IV_c type, halite, and sylvite daughter mineral-bearing inclusions with negative crystal shape (from Yulong); h. IV_c type, opaque, halite and calcite daughter mineral-bearing inclusions (from Yulong); i. The fluid inclusion assemble of boiling (from Yulong); j. I–type SMI (from Beiya).

Fig. 2a, j). All the SMI are crystallized with round or irregular shape. It consists of glass, bubble, crystalline aggregates (such as quartz, feldspar), and occur along the growth zone or isolated in the quartz phenocryst. The diameters of most SMI are between 5 and 30 μm. The Fig. 3 shows the original room temperature phenomenon and after homogenization phenomenon of the I-type SMI.

II-type: NaCl-H_2O inclusions (Fig. 2e). These are two-phase aqueous inclusions, consisting of vapor and liquid water at room temperature,

Fig. 3. (a) I-type SMI in room temperature (25 ℃); (b) after homogenization (about 810 ℃). The scale is 10 μm (sample from Beiya).

and they can be divided into three subtypes according to their vapor to liquid ratio: II_a, the liquid occupies > 70 vol% of the inclusion; II_b, the liquid occupies between 30 and 70 vol% of the inclusion; II_c, the liquid occupies < 30 vol% of the inclusion. These fluid inclusions usually have oval or irregular shapes, with a few negative crystal shapes. They occur in isolation or cluster along healed crystal fissures or growth zones.

III-type: CO_2-rich fluid inclusions. There are three-phase at room temperature (V_{CO2} + L_{CO2} + L_{H2O}) in III-type fluid inclusion and have round or oval shapes (Fig. 2b).They can be subdivided into III_a and III_b subtypes. III_a, contains both H_2O and CO_2 (V_{CO2} + L_{CO2} + L_{H2O}). III_b (Fig. 2c), contains H_2O, CO_2 and an opaque daughter-mineral (V_{CO2} + L_{CO2} + L_{H2O} + opaque daughter-mineral).

IV-type: Daughter mineral-bearing inclusions without CO_2. They can be subdivided into IV_a, IV_b, IV_c and IV_d subtypes. IV_a, consists of a liquid and a vapor phase plus a halite daughter mineral and the liquid occupies above 50 vol% of the inclusion (Fig. 2d). IV_b, consists of a liquid and a vapor phase plus an opaque daughter mineral and the liquid occupies < 30 vol% of the inclusion (Fig. 2f). IV_c, consists of a liquid and a vapor phase plus crystals of different daughter minerals such as halite, sylvite, calcite and an opaque phase (Fig. 2g, h).

3.2. Inclusions assemblages in the quartz phenocryst of five porphyry rocks

IV-type daughter mineral-bearing inclusions (approximately 85%) inclusions are dominant in the quartz phenocryst of the Yulong quartz monzonite porphyry. Also, some II-type NaCl-H_2O fluid inclusions (approximately 10%) and a few I-type SMI (< 5%) in the quartz phenocryst. CO_2 phase in the fluid inclusions are visible at room temperature and only can be test during the microscopic temperature measuring experiment. The IV-type fluid inclusions consist of IV_a (approximately 10%), IV_b (approximately 35%), and IV_c (approximately 40%) subtypes. Most of the fluid inclusions contain halite, sylvite, calcite and opaque daughter minerals. The diameters of fluid inclusions are between 10 and 25 μm and the inclusions are round or negative crystal shapes. SMI can only be observed in a few quartz phenocrysts, and are usually crystallized with round shape and the size is < 10 μm.

Four types of inclusions can be observed in the quartz phenocrysts of the granite porphyry of Machangqing. I-type (approximately 15%) SMI are usually crystallized and occur along the growth zone of the quartz phenocrysts. II-type (approximately 10%) are NaCl-H_2O inclusions. III-type (approximately 20%) CO_2-rich fluid inclusions are III_a-subtype with three phase at room temperature (V_{CO2} + L_{CO2} + L_{H2O}) and have round or oval shapes. IV-type (approximately 55%) inclusions consist of mainly IV_a (approximately 20%), IV_b (approximately 15%), and IV_c (approximately 20%) subtypes. The diameters both of fluid inclusions and SMI in the Machangqing deposit are commonly < 10 μm.

Inclusions in the quartz phenocrysts of the quartz syenite porphyry of Tongchang are too small to study (approximately 10 μm). They are mainly IV-type (approximately 50%), III-type inclusions (approximately 30%) and II-type (approximately 15%) inclusions. I-type(< 5%) SMI are rarely observed. II-type are NaCl-H_2O inclusions. III-type CO_2-rich fluid inclusions are dominantly the III_b-subtype, with multi-phase at room temperature (V_{CO2} + L_{CO2} + L_{H2O} + opaque daughter-mineral), and show round or oval shapes. IV-type are mainly including the IV_a (approximately 20%), IV_b (approximately 10%), and IV_c (approximately 20%) subtypes.

Four types of inclusions have been observed in the quartz phenocrysts of the Beiya quartz syenite porphyry. I-type (approximately 10%) SMI are usually crystallized and occur in or along the growth zone of the quartz phenocrysts. II-type (approximately 10%) are NaCl-H_2O inclusions. III-type (approximately 10%) CO_2-rich fluid inclusions are the III_a-subtype with three phases at room temperature (V_{CO2} + L_{CO2} + L_{H2O}) and have round or oval shapes. IV-type (approximately 70%) are mainly including the IV_a (approximately 30%), IV_b (approximately 30%), and IV_c (approximately 10%) subtypes. The diameters of both fluid inclusions and SMI of the Beiya are commonly < 15 μm.

Inclusions in quartz phenocrysts of the Yanshuiqing quartz syenite porphyry are mainly I-type SMI (> 95%), and with a few II-type inclusions (< 5%). The SMI are crystallized and occur along the growth zone of the quartz. The diameters of most SMI are between 15 and 30 μm, and fluid inclusions are between 10 and 20 μm. The SMI are crystallized and opaque at room temperature, suggest that the Yanshuiqing quartz syenite porphyry are cooling slowly.

3.3. The contrast of inclusions in quartz phenocryst and vein quartz

In contrast, SMI in the quartz phenocrysts of the ore-bearing porphyries are fewer, but fluid inclusions in both quartz phenocryst and vein quartz of the ore-bearing porphyries are abundant. There are two possible reasons for this phenomenon: 1, Quartz phenocrysts were crystallized from the fluid phase, but there is no clear evidence to support that phenocryst minerals of the porphyry crystallized from the fluid phase, they mostly crystalized from magma; and 2, Fluid inclusions in quartz phenocrysts are mostly secondary inclusions except some of them are primary inclusions that were trapped as soon as a fluid phase coexists with the silicate melt.

As mentioned above, fluid inclusions in the quartz phenocryst of the Yulong quartz monzonite porphyry and vein quartz are abundant and easily recognizable, thus were chosen for microthermometry studies (Figs. 4 and 5). Approximately 120 fluid inclusions were measured using a Linkam THMSG 600 heating-freezing stage in the State Key

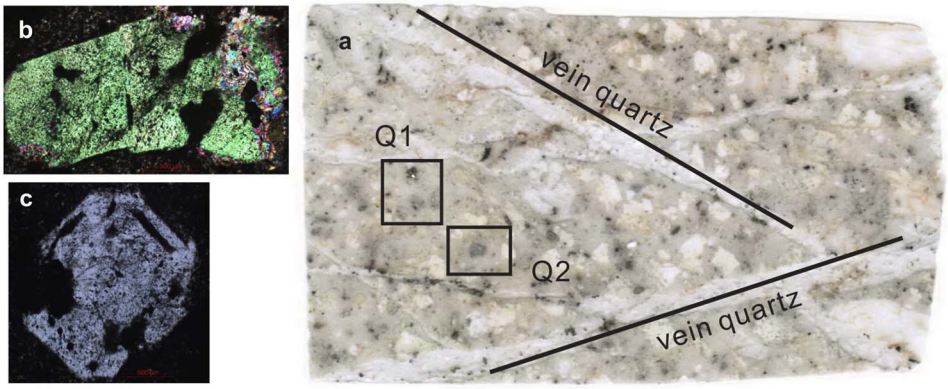

Fig. 4. (a) The scanning image of the sample YL911-1 (Yulong); (b) phenocryst quartz (Q1); (c) phenocryst quartz (Q2).

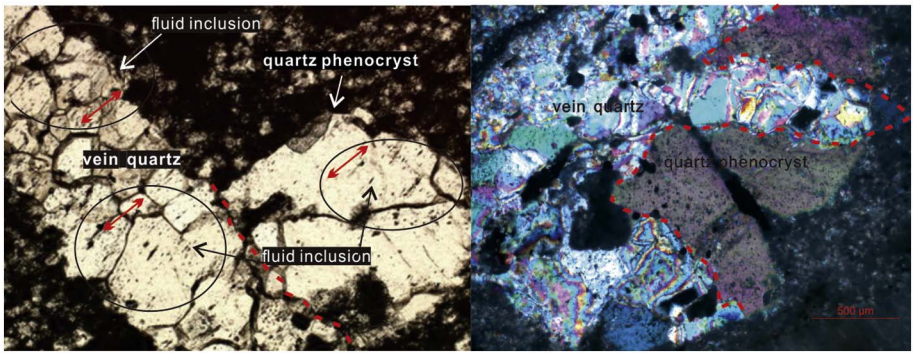

Fig. 5. On the left: the long axis direction of fluid inclusions (within the ellipse) both in the quartz phenocryst and vein quartz are growth along a preferred orientation (as the red arrow point to); on the right: how the quartz phenocryst is cut by the vein quartz. The red dotted line shows the boundary of quartz phenocryst and vein quartz. (For interpretation of the references to colour in this figure legend, the reader is referred to the web version of this article.)

Laboratory of ore deposit geochemistry, Institute of Geochemistry, Chinese Academy of Sciences. Only 83 inclusions have valid data in the Table 1 because some fluid inclusions are explosed before homogenization. The heating/freezing rate was run generally 0.2–5 °C/min, but was reduced to < 0.2 °C/min near the phasetrans formation. The salinities of the NaCl-H_2O inclusions were calculated according to the freezing temperature of ice and using an equation provided by Bodnar (1993). The salinities of the NaCl-H_2O-CO_2 inclusions were calculated according to the melting of CO_2 clathrate (Roedder, 1971).

Fluid inclusions both in the quartz phenocrysts and the vein quartz of the Yulong deposit were studied. The results show that the types of inclusions in the two types of quartz are relatively consistent: both with daughter mineral (including opaque daughter mineral)-bearing fluid inclusions, the vapor-rich inclusions, and the gas-liquid inclusions. Furthermore, temperature and salinity measurements show that inclusions in the two types of quartz have similar temperatures and salinity (Table 1 and Fig. 6). The range of the salinity and homogenization temperature in the quartz phenocrysts is wider than in the vein quartz, which could be the result of a mixture of several period of fluids. Petrographic observation shows that the long axis direction of fluid inclusions both in the quartz phenocryst and vein quartz are growth along the same orientation, and the quartz phenocryst was cut by the vein quartz (Fig. 5), suggest that the forming of fluid inclusions in the quartz phenocrysts may have a relationship with the vein quartz.

Table 1
The characteristics of the inclusions (size, number, type etc.) and the microthermometry results for the vein quartz and phenocrysts ('Size' in the table means the length of long axis direction of the fluid inclusion). T (m, CO_2): the triple point temperature of the carbon dioxide. T (m, ice): the melting temperature of the ice. T (m, clath): the melting temperature of the carbon dioxide hydrate; T (h, CO_2): the partial homogenization temperature of the carbon dioxide. T (m, NaCl): the melting temperature of the halite. Tm, calcite: the melting temperature of the calcite. T (h, total): the total homogenization temperature. W_{NaCl}/wt%: the salinity of the fluid inclusion.

YL	Type	Shape	Size (μm)	T (m, CO_2)	T (m, ice)	T (m, clath)	T (h, CO_2)	T (m, NaCl)	T (m, calcite)	T (h, total)	W_{NaCl}/wt%
Quartz phenocryst	L + V	Xenomorphic	20		− 8.9					202	12.7
	L + V	Xenomorphic	9		− 5.9					239	9.1
	L + V + M	Hypautomorphic	18		− 7.9					490	11.6
	L + V + M	Negative	18		− 10					487	13.9
	L + V + M	Xenomorphic	22.4		− 15.3					441	18.9
	L + V + M	Irregular	17.5		− 8.9					430	12.7
	L + V + M	Xenomorphic	16		− 7.4					456	11.0
	L + V + M	Xenomorphic	17		− 7.6					460	11.2
	L + V + M	Xenomorphic	22		− 19.6					> 550	22.1
	L + V + NaCl	Negative	11.4					242		297	34.2
	L + V + NaCl	Negative	10.2					374		374	44.7
	L + V + NaCl + M	Negative	10					305		305	38.6
	L + V + NaCl + M	Negative	11					344		344	41.9
	L + V + NaCl + M	Negative	9.6					330		330	40.6
	L + V + NaCl + M	Negative	11.2					276		317	36.4
	L + V + NaCl + M	Negative	8.1					339		339	41.4
	L + V + NaCl + M	Negative	11.2					226		310	33.3
	L + V + NaCl + M	Negative	8					320		320	39.8
	L + V + NaCl + M	Negative	8.8					325		325	40.2
	L + V + NaCl + calcite + M	Negative	15					305	319	383.5	38.6
	L + V + NaCl + calcite + M	Irregular	15					319	411	411	39.7
	L + V + NaCl + calcite + M	Irregular	12					332	401	401	40.8
	L + V + NaCl + calcite + M	Irregular	15					307	About 380	380	38.7
	L + V + NaCl + calcite + M	Xenomorphic	9.5					226	248	325	33.3
	$L(H_2O)$ + $L(CO_2)$ + V (CO_2)	Xenomorphic	18.5	− 55.7		7.1	16.3			289	5.5
	$L(H_2O)$ + $L(CO_2)$ + V (CO_2)	Xenomorphic	28	− 55.7		6	16.1			430	7.4

(*continued on next page*)

Table 1 (*continued*)

YL	Type	Shape	Size (μm)	T (m, CO_2)	T (m, ice)	T (m, clath)	T (h, CO_2)	T (m, NaCl)	T (m, calcite)	T (h, total)	W_{NaCl}/wt%
Vein quartz	L + V	Round	7		− 5.6					295	8.7
Vein quartz	L + V	Xenomorphic	13.4		− 20.6					343	22.8
	L + V + M	Xenomorphic	8		− 13.5					346	17.3
	L + V + M	Oval	15	− 55.5		5.6	16.3			378	8.0
	L + V + M	Oval	10	− 55.6		6.2	19.9			368	7.1
	L + V + M	Oval	8.7	− 55.6		5.9	16.1			421	7.5
	L + V + M	Negative	13		− 11.7					439	15.7
	L + V + M	Negative	16.8		− 13.8					> 600	17.6
	L + V + M	Negative	18.7		− 14.7					> 600	18.4
	L + V + M	Negative	16.7		− 13.3					> 600	17.2
	L + V + M	Oval	20.4		− 10.4					390	14.4
	L + V + M	Negative	12.3	− 55.9		7.1	About 20.9			350	5.5
	L + V + NaCl + M	Negative	12					352		352	42.6
	L + V + NaCl + M	Negative	12					355		355	42.9
	L + V + NaCl + M	Irregular	14					332		332	40.8
	L + V + NaCl + M	Strip	17					266		325	35.7
	L + V + NaCl + M	Negative	12					295		304	37.8
	L + V + NaCl + M	Negative	11.7					309		309	38.9
	L + V + NaCl + M	Negative	7.3					315		315	39.4
	L + V + NaCl + M	Negative	7.5					228		298	33.4
	L + V + NaCl + M	Negative	13.6					313		328.4	39.2
	L + V + NaCl + M	Negative	8.6					155		344	29.9
	L + V + NaCl + M	Negative	4					340		348	41.5
	L + V + NaCl + M	Negative	6					310		310	39.0
	L + V + NaCl + M	Xenomorphic	17.7					283		383	36.9
	L + V + NaCl + M	Xenomorphic	9.1					278		325	36.5
	L + V + NaCl + M	Negative	8					287		287	37.2
	L + V + NaCl + M	Negative	8					289		289	37.3
	L + V + NaCl + M	Negative	11.7					320		320	39.8
	L + V + NaCl + M	Negative	8.5					241		337	34.1
	L + V + NaCl + M	Negative	7.8					327		327	40.4
	L + V + NaCl + M	Negative	9.8					316		316	39.4
	L + V + NaCl + M	Negative	10.1					234		371	33.7
	L + V + NaCl + M	Negative	10.8					210		383	32.4
	L + V + NaCl + M	Negative	9.3					199		256	31.8
	L + V + NaCl + M	Negative	9.3					239		382	34.0
	L + V + NaCl + M	Negative	10.3					327		327	40.4
	L + V + NaCl + M	Negative	8.2					360		360	43.4
	L + V + NaCl + M	Negative	7					350		350	42.4
	L + V + NaCl + M	Negative	9.6					304		304	38.5
	L + V + NaCl + M	Negative	7.3					314		314	39.3
	L + V + NaCl + M	Negative	11.3					319		319	39.68
	L + V + NaCl + calcite + M	Negative	12.6					372		423	44.5
	L + V + NaCl + calcite + M	Negative	14					308		308	38.8
	L + V + NaCl + calcite + M	Negative	10					305		305	38.6
	L + V + NaCl + calcite + M	Negative	8					364		364	43.7
	L + V + NaCl + calcite + M	Triangle	10.2					352	356	356	42.6
	L + V + NaCl + calcite + M	Square	13.6					348	358	358	42.2
	$L(H_2O) + L(CO_2) + V(CO_2) + M$	Xenomorphic	26.2				20.9			142	–
	$L(H_2O) + L(CO_2) + V(CO_2) + M$	Xenomorphic	30	− 55.8		− 8.6	19.9				21.1

Therefore, the fluid inclusions in the phenocrysts mostly belong to the secondary inclusions that formed when the metasomatism of hydrothermal fluid to the porphyry rock occurred. In addition, some of the fluid inclusions in the phenocrysts are primary inclusions that were trapped as soon as a fluid phase coexists with the silicate melt (Frezzotti, 2001; Harris et al., 2003; Kamenetsky et al., 1999; Thomas et al., 2000).

3.4. Fluid inclusion microthermometry work of some typical Cu (Au, Mo) deposits

The microthermometric studies were conducted on Yulong, Beiya and Tongchang deposits (Figs. 7 and 8). II-type and IVa-subtype inclusions were homogenized to the liquid phase or vapor phase, and the salinities calculation yielded to the ice-melting temperatures ($T_{m,ice}$).

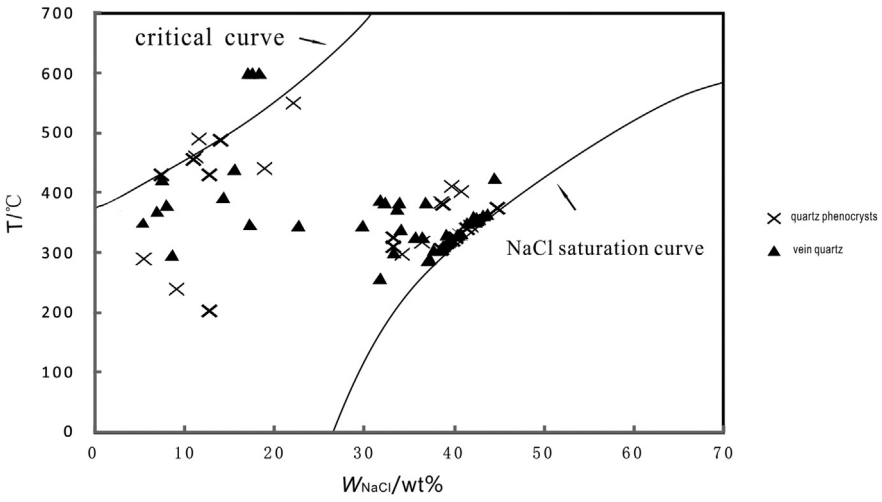

Fig. 6. The results of the microthermometry analyses of inclusions in quartz phenocrysts and vein quartz from the Yulong deposit.

III-type inclusions were homogenized to the liquid phase, and the salinities calculation depended on the melting of CO_2 clathrate ($T_{m,clath}$). IV-type inclusions were homogenized to the liquid phase, and the salinities calculation yielded to the dissolution temperatures of halite ($T_{m,NaCl}$).

The fluid inclusions in Yulong deposit finally homogenized at temperatures of 220–480 ˚C, some over 600 ˚C. The salinity of mineralizing solutions manifests bimodal distribution pattern with two ranges from 2 to 22 wt% NaCl equivalent and from 28 to 46 wt% NaCl equivalent.

The fluid inclusions in Beiya deposit finally homogenized at temperatures of 220–520 ˚C. The salinity of mineralizing solutions also manifests bimodal distribution pattern with two ranges from 2 to 24 wt % NaCl equivalent and from 32 to 44 wt% NaCl equivalent.

The fluid inclusions in Tongchang deposit finally homogenized at temperatures of 240–460 ˚C. The salinity of mineralizing solutions also manifests bimodal distribution pattern with two ranges from 2 to 22 wt % NaCl equivalent and from 30 to 52 wt% NaCl equivalent.

4. Discussion

In this study, fluid inclusion petrography and microthermometry were carried out in detail on several porphyry rocks. The results show that the characteristics of fluid inclusions assemblages in ore-bearing and barren alkali-rich rocks are distinct: inclusions in minerals from the Yanshuiqing barren rocks are dominated by the primary silicate melt inclusions, whereas fluid inclusion is rare. In contrast, inclusions in minerals from ore-bearing porphyries (Yulong, Machangqing, Beiya, Yao'an and Tongchang) are mainly fluid inclusions, with minor SMI. The further percentage estimates for each type of inclusions in ore bearing and barren porphyries are given in the pie diagrams (Fig. 9) for an intuitive perspective of the occurrence of fluid inclusion types and their abundance.

Halite, sylvite, calcite and an opaque phase daughter minerals bearing fluid inclusions from ore-bearing rocks are common but rare in fluid inclusions from barren rocks. Furthermore, the mostly opaque phase daughter minerals in the Yulong deposit are proven to be chalcopyrite (Xie et al., 2005), which suggests that the fluid inclusions with opaque phase daughter minerals are rich in copper. Similarly, the type of inclusions in quartz phenocrysts from other porphyry deposits (e.g., Bingham, El Teniente, Bajo de la Alumbrera, Butte, Grasberg) are dominated by fluid inclusions especially the fluid inclusions with halite, sylvite, calcite daughter mineral and an opaque phase but contain fewer silicate melt inclusions (Harris et al., 2005; Klemm et al., 2007; Roedder, 1971; Rusk et al., 2004; Ulrich et al., 1999).

Fluid inclusion petrography and microthermometry show that the ore forming fluids of this study belong to the H_2O-NaCl ± CO_2 system with high temperature (250–500 ˚C) and high salinity (10–50 wt% NaCl equivalent). Which means that the ore-forming fluid has the characteristics of high temperature, high salinity, and points to a typical magmatic-hydrothermal fluid (Figs. 7 and 8). Furthermore, the coexisting of vapor rich inclusions and halite-bearing fluid inclusion and their similar homogenization temperatures suggested that the boiling of the hydrothermal fluid (Fig. 2i shows the fluid inclusions assemblages of boiling). Also, the boiling phenomenon were observed in many other porphyry Cu (Mo, Au) deposit (Ulrich et al., 1999; Harris et al., 2005; Klemm et al., 2007; Ni et al., 2015; Wang et al., 2015; Li et al., 2015), occurred during the ore stage and probably promoted a rapid precipitation of copper, gold and molybdenite.

Hydrous mineral such as amphibole, biotite and apatite are common in the alkaline intrusions of the Jinshajiang–Red River alkali-rich intrusive belt but difference on the content. Table 2 is the roughly content of minerals in the studied rocks. It shows that the content of amphibole and biotite in Cu (Mo, Au)-mineralized alkaline intrusions are more than barren rocks. It suggests that the volatile amount in the magma of Cu (Mo, Au)-mineralized and barren alkaline intrusions are difference and the former are richer in water. Besides, according to the sample describe, all of the samples from Cu (Au, Mo)-mineralized porphyry are underwent K-silicate and phyllicalteration, but samples from barren porphyry are more fresh. Both of them are response to the result of fluid inclusion petrography and suggest the differences of volatile between the mineralized and barren alkaline intrusions. The researcher on apatite and fluid inclusions also demonstrates that water and metal elements are richer in mineralization-related porphyry than barren porphyry(Audetat et al., 2008; Rasmussen and Mortensen, 2013), which indicates that the ore-bearing rocks are richer in H_2O, K, Na, Ca and metal elements (especially Cu, Au, Mo, Fe, Zn, etc.) than the barren rocks.

The study of the Yulong deposit provides some clues to explain the contrasting features of fluid inclusions in ore-bearing and barren alkali-rich rocks. It shows that the fluid inclusions in the porphyry minerals are mostly secondary fluid inclusions, although some of the fluid inclusions are primary inclusions which trapped coexisting with the silicate melt (Frezzotti, 2001; Harris et al., 2003; Kamenetsky et al., 1999; Thomas et al., 2000). In any case, it suggests that the ore-bearing rocks

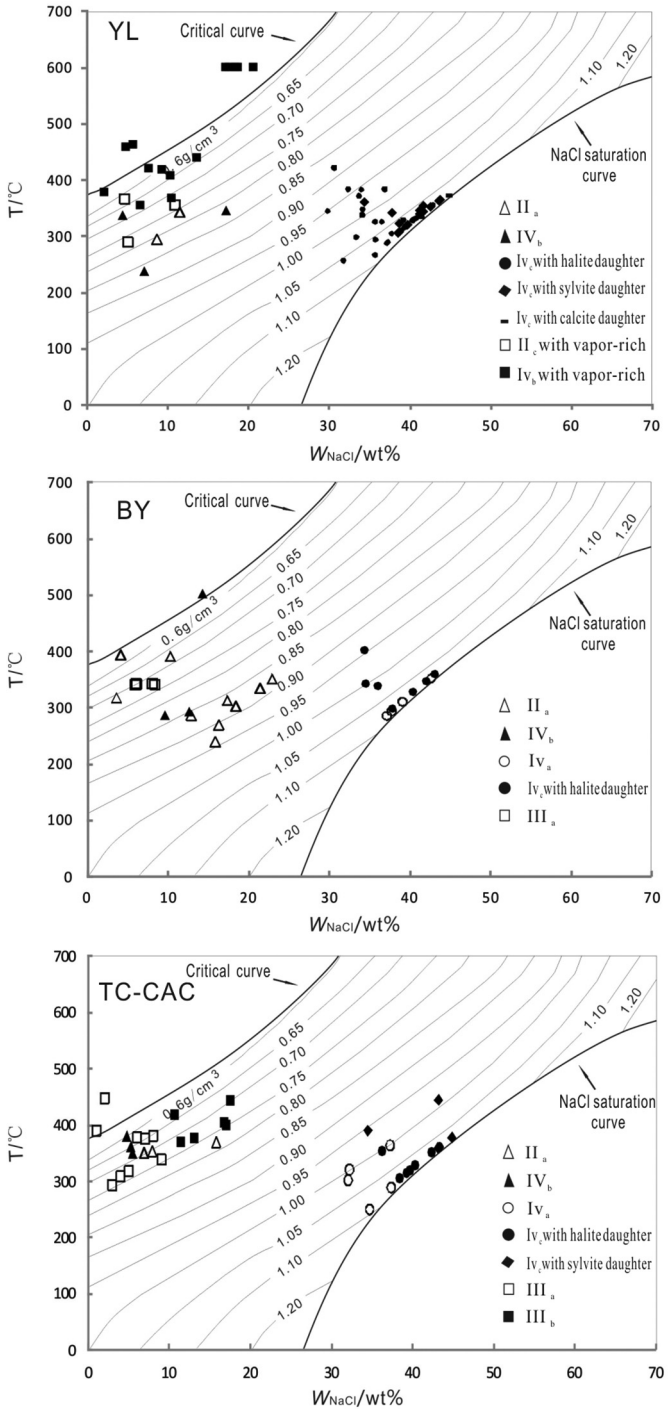

Fig. 7. Th-W_{NaCl}-ρ of ore deposit fluid in Yulong (YL), Beiya (BY) and Tongchang (TC) deposit.

were formed from water-rich magma or were extensively metasomatized by the magmatic hydrothermal fluid, and the barren rocks were water-lack or were weakly metasomatized by fluids.

Therefore, the degree of development of fluid inclusions especially the fluid inclusions with halite, sylvite, calcite and an opaque phase daughter mineral in the quartz phenocryst correlates positively with the degree of rock mass transformed by hydrothermal fluid.

Water (H_2O) is a vital factor in the formation of magmatic-hydrothermal deposits (Bai and Koster van Groos, 1999; Candela and Piccoli, 1995; Candela, 1997). Copper and other ore metals are considered to have been extracted from the silicate melt when magmatic hydrothermal fluids exsolved from the magma during crystallization and decompression processes (Burnham and Ohmoto, 1979; Burnham, 1997; Hedenquist and Lowenstern, 1994).The metals were precipitated later within and around the pluton as the magmatic fluids cooled and mix with externally derived fluids. A number of fluid inclusion studies have demonstrated that ore-forming fluids in porphyry systems are characterized by high temperature and high salinity, which is reflected in inclusions that contain halite, sylvite and an opaque daughter minerals (Harris et al., 2005; Klemm et al., 2007; Roedder, 1971; Rusk et al., 2004; Ulrich et al., 1999). Therefore, the number and type of fluid inclusions in the phenocrysts, especially high salinity with an opaque mineral could be used to indicate the potential of porphyry copper, gold and molybdenite deposits.

5. Conclusion

Fluid inclusion petrography and microthermometry studies of barren and mineralized porphyry intrusions from the Jinshajiang–Red River alkali-rich intrusive belt was carried out in detail. The results show that:

1) The fluid inclusions assemblages in ore-bearing and barren porphyries are distinct. Inclusions in minerals from barren porphyry are dominated by the primary silicate melt inclusions, contain rare fluid inclusions, whereas inclusions in minerals from ore-bearing porphyries are mainly dominated by fluid inclusions, with minor silicate melt inclusions. The approximate percentage estimate of the silicate melt inclusions in Yulong, Machangqing, Tongchang, Beiya and Yanshuiqing are 5%, 15%, 5%, 10%, 95%, respectively.
2) The fluid inclusions in the porphyry minerals are mostly secondary fluid inclusions, although some of the fluid inclusions are primary inclusions which trapped coexists with the silicate melt. It suggests that the ore-bearing rocks were formed from water-rich magma or were extensively metasomatized by the magmatic hydrothermal fluid, and the barren rocks are water-lack or were weakly metasomatized by fluids.
3) The study suggested that the degree of development of fluid inclusions especially the fluid inclusions with halite, sylvite, calcite and an opaque phase daughter minerals in the quartz phenocryst, correlates positively with the degree of rock mass transformed by hydrothermal fluid and could be regarded as an indication of the metallogenic potential of a porphyry system.

Acknowledgements

We are grateful to professor Ni Pei, Thomas Ulrich and Niu Hecai for greatly improved the manuscript and thanks to the editors. This research project is financially supported jointly by ‘the Key Natural Science Foundation of China’ (41130423) and ‘the Natural Science Foundation of China’ (41502087).

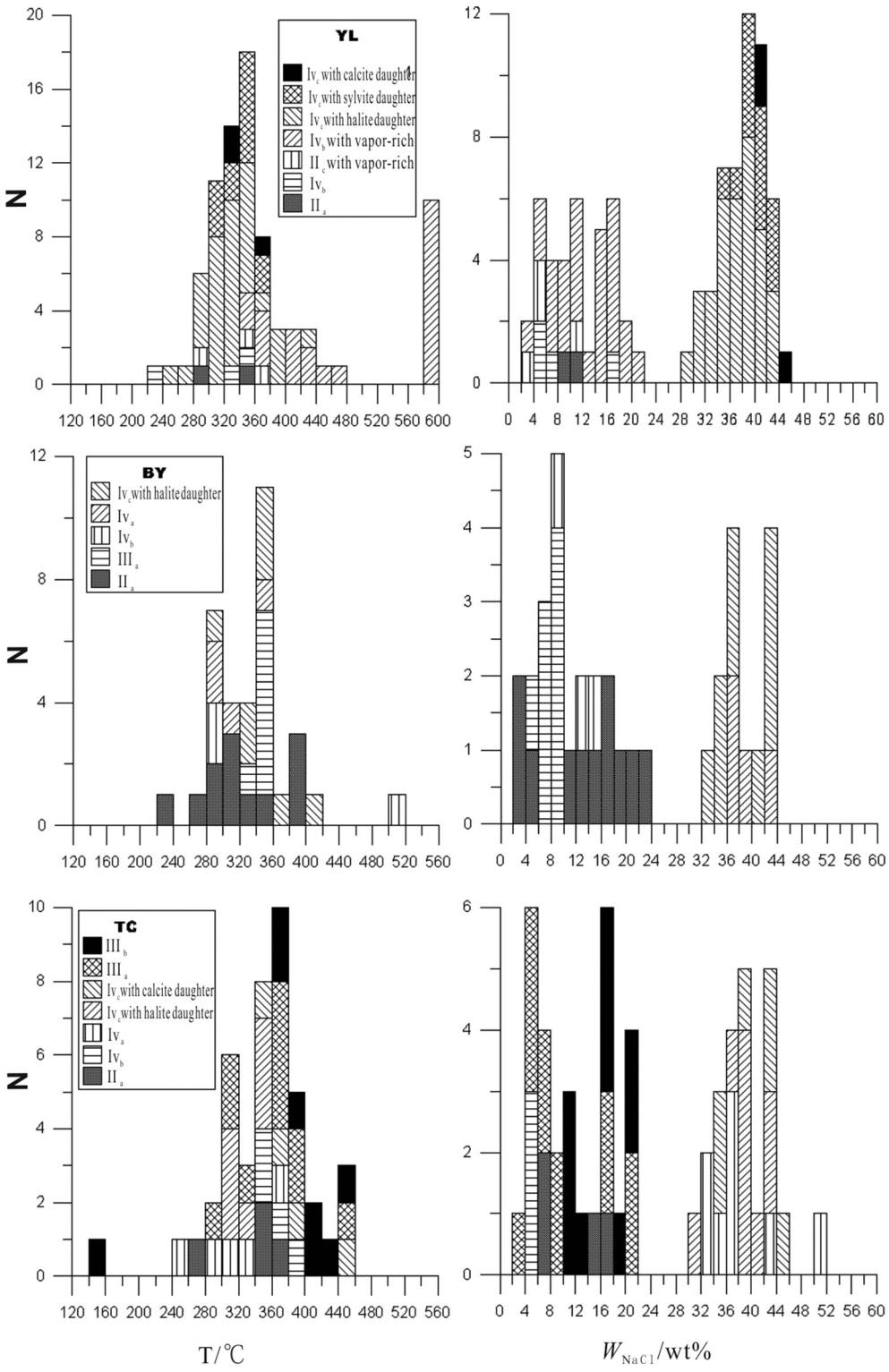

Fig. 8. T/°C and salinity (wt% NaCleq) of ore deposit fluid in Yulong (YL), Beiya (BY) and Tongchang (TC) deposit.

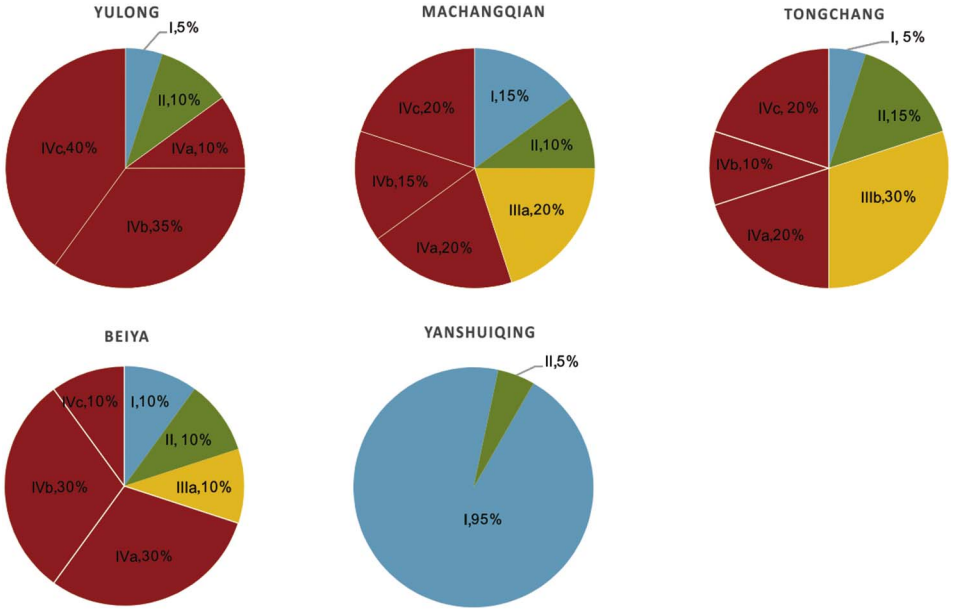

Fig. 9. Pie diagrams illustrating the occurrence of fluid inclusion types and their abundance. I: Silicate melt inclusions. II: NaCl-H_2O inclusions with two-phase aqueous inclusions. III_a, contains both H_2O and CO_2 (V_{CO2} + L_{CO2} + L_{H2O}). III_b, contains H_2O, CO_2 and an opaque daughter-mineral (V_{CO2} + L_{CO2} + L_{H2O} + opaque daughter-mineral). IV_a, consists of a liquid and a vapor phase plus a halite daughter mineral and the liquid occupies above 50 vol% of the inclusion. IV_b, consists of a liquid and a vapor phase plus an opaque daughter mineral and the liquid occupies < 30 vol% of the inclusion. IV_c, consists of a liquid and a vapor phase plus crystals of different daughter minerals such as halite, sylvite, calcite and an opaque phase.

Table 2
The general statistics of the main minerals in the studied rock. '–'means none; '+'means less; '++'means more.

Alkaline intrusions	K-feldspar	Plagioclase	Pyroxene	Amphibole	Biotite
Quartz monzonite porphyry of Yulong	+	++	–	+	++
Granite porphyry of Machangqing	+	++	–	++	++
Quartz syenite porphyry of the Tongchang	++	++	–	++	++
Quartz syenite porphyry of the Beiya	++	+	–	+	++
Quartz syenite porphyry of Yanshuiqing	++	+	+	+	+

References

Audetat, A., Gunther, D., Heinrich, C.A., 1998. Formation of a magmatic-hydrothermal ore deposit: insights with LA-ICP-MS analysis of fluid inclusions. Science 279 (5359), 2091–2094.

Audetat, A., Pettke, T., Heinrich, C.A., Bodnar, R.J., 2008. The composition of magmatic-hydrothermal fluids in barren and mineralized intrusions. Econ. Geol. 103 (5), 877–908.

Bai, T.B., Koster van Groos, A.F., 1999. The distribution of Na, K, Rb, Sr, Al, Ge, Cu, W, Mo, La, and Ce between granitic melts and coexisting aqueous fluids. Geochim. Cosmochim. Acta 63 (7), 1117–1131.

Bi, X.W., Hu, R.Z., Cornell, D.H., 2002. The origin of altered fluid: REE evidence from primary and secondary feldpars in the mineralization zone. Ore Geol. Rev. 19, 69–78.

Bi, X.W., Hu, R.Z., Cornell, D.H., 2004. The alkaline porphyry associated Yao'an gold deposit, Yunnan, China: rare earth element and stable isotope evidence for magmatic-hydrothermal ore formation. Mineral. Deposita 39 (1), 21–30.

Bi, X.W., Hu, R.Z., Peng, J.T., Wu, K.X., Su, W.C., Zhang, X.Z., 2005. Geochemical characteristics of the Yao'an and Machangqing alkaline-rich intrusions. Acta Petrol. Sin. 21 (01), 0113–0124 (in Chinese).

Bi, X.W., Hu, R.Z., Hanley, J.J., Mungall, J.E., Peng, J.T., Shang, L.B., Wu, K.X., Shuan, Y., Li, H.L., Hu, X.Y., 2009. Crystallisation conditions (T, P, fO_2) from mineral chemistry of Cu- and Au-mineralised alkaline intrusions in the Red River–Jinshajiang alkaline igneous belt,western Yunnan Province, China. Mineral. Petrol. 96, 43–58.

Bodnar, R.J., 1993. Revised equation and stable for determining the freezing point depression of H_2O-NaCl solutions. Geochim. Cosmochim. Acta 57, 683–684.

Burnham, C.W., 1997. Magmas and hydrothermal fluids. In: Barnes, H.L. (Ed.), Geochemistry of Hydrothermal Ore Deposits. Wiley, New York, pp. 63–118.

Burnham, C.W., Ohmoto, H., 1979. Late-stage processes of felsic magmatism. Min. Geol. Spec. Issue 8, 1–11.

Candela, P.A., 1997. A review of shallow, ore-related granites: textures, volatiles, and ore metals. J. Petrol. 38 (12), 1619–1633.

Candela, P.A., Piccoli, P.M., 1995. Model ore-metal partitioning from melts into vapor and vapor/brine mixtures. Magmas Fluids Ore Depos. 23, 101–127.

Chung, S.L., Lee, T.Y., Lo, C.H., Wang, P.L., Chen, C.Y., Yem, N.T., Hoa, T.T., Wu, G.Y., 1997. Intraplate extension prior to continental extrusion along the Ailao Shan-Red River shear zone. Geology 25 (4), 311–314.

Chung, S.L., Lo, C.H., Lee, T.Y., Zhang, Y.Q., Xie, Y.W., Li, X.H., Wang, K.L., Wang, P.L., 1998. Diachronous uplift of the Tibetan plateau starting 40 Myr ago. Nature 394, 769–773.

Cooke, D.R., Hollings, P., Walsh, J.L., 2005. Giant porphyry deposits: characteristics, distribution, and tectonic controls. Econ. Geol. 100 (5), 801–817.

Frezzotti, M.L., 2001. Silicate-melt inclusions in magmatic rocks: applications to petrology. Lithos 55 (1–4), 273–299.

Gu, X.X., Tang, J.X., Wang, C.S., Chen, J.P., He, B.B., 2003. Himalayan magmatism and porphyry copper-molybdenum mineralization in the Yulong ore belt, East Tibet. Mineral. Petrol. 78 (1–2), 1–20.

Halter, W., Heinrich, A.C., Pettke, T., 2005. Magma evolution and the formation of porphyry Cu-Au ore fluids: evidence from silicate and sulfide melt inclusions. Mineral. Deposita 39 (8), 845–863.

Harris, A.C., Kamenetsky, V.S., White, N.C., van Achterbergh, E., Ryan, C.G., 2003. Melt inclusions in veins: linking magmas and porphyry Cu deposits. Science 302 (19), 2109–2111.

Harris, A.C., Golding, S.D., White, N.C., 2005. Bajo de la Alumbrera copper-gold deposit: stable isotope evidence for a porphyry-related hydrothermal system dominated by magmatic aqueous fluids. Econ. Geol. 100 (5), 863–886.

Hedenquist, J.W., Lowenstern, J.B., 1994. The role of magmas in the formation of hydrothermal ore deposits. Nature 370, 519–527.

Hou, Z.Q., Ma, H.W., Zaw, K., Zhang, Y.Q., Wang, M.J., Wang, Z., Pan, G.T., Tang, R.L., 2003. The Himalayan Yulong porphyry copper belt: product of large-scale strike-slip faulting in eastern Tibet. Econ. Geol. Bull. Soc. Econ. Geol. 98 (1), 125–145.

Hou, Z.Q., Zeng, P.S., Gao, Y.F., Du, A., Fu, D.M., 2006. Himalayan Cu-Mo-Au mineralization in the eastern Indo-Asian collision zone: constraints from Re-Os dating of molybdenite. Mineral. Deposita 41, 33–45.

Hou, Z.Q., Pan, X.F., Yang, Z.M., Qu, X.M., 2007. Porphyry Cu-(Mo-Au) deposits no related to oceanic-slab subduction: examples from Chinese porphyry deposits in continental settings. Geoscience 21 (2), 332–351 (in Chinese).

Hu, R.Z., Burnard, P.G., Turner, G., Bi, X.W., 1998. Helium and argon isotope systematics in fluid inclusions of Machangqing copper deposit in west Yunnan province, China. Chem. Geol. 146, 55–63.

Hu, R.Z., Burnard, P.G., Bi, X.W., Zhou, M.F., Pen, J.T., Su, W.C., Wu, K.X., 2004. Helium and argon isotope geochemistry of alkaline intrusion-associated gold and copper deposits along the Red River–Jinshajiang fault belt, SW China. Chem. Geol. 203 (3–4), 305–317.

Jiang, Y.H., Jiang, S.Y., Ling, H.F., Dai, B.Z., 2006. Petrogencesis of Cu-bearing porphyry associated with continent-continent collisional setting: evidence from the Yulong porphyry Cu ore-belt, east Tibet. Acta Petrol. Sin. 22 (3), 697–706 (in Chinese).

Kamenetsky, V.S., Wolfe, R.C., Eggins, S.M., Mernagh, T.P., Bastrakov, E., 1999. Volatile solution at the Inkidi Cu-Au porphyry deposit, Philippines: a melt-inclusion record of the initial ore-forming process. Geology 27, 691–694.

Klemm, L.M., Pettke, T., Heinbicth, C.A., Campos, E., 2007. Hydrothermal evolution of the El Teniente deposit, Chile: porphyry Cu-Mo ore deposition from low-salinity magmatic fluids. Econ. Geol. 102 (6), 1021–1045.

Li, L., Ni, P., Wang, G.G., Zhu, A.D., Pan, J.Y., Chen, H., Huang, B., Yuan, H.X., Wang, Z.K., Fang, M.H., 19 November 2015. Multi-stage fluid boiling and formation of the giant Fujiawu porphyry Cu–Mo deposit in South China. Ore Geol. Rev (Available online).

Liang, H.Y., Campbell, I.H., Allen, C., Sun, W.D., Liu, C.Q., Yu, H.X., Xie, Y.W., Zhang, Y.Q., 2006. Zircon Ce^{4+}/Ce^{3+} ratios and ages for Yulong ore-bearing porphyries in eastern Tibet. Mineral. Deposita 41 (2), 152–159.

Liang, H.Y., Campbell, I.H., Allen, C.M., Sun, W.D., Yu, H.X., Xie, Y.W., Zhang, Y.Q., 2007. The age of the potassic alkaline igneous rocks along the Ailao Shan-Red River shear zone: implications for the onset age of left-lateral shearing. J. Geol. 115 (2), 31–242.

Liang, H.Y., Sun, W.D., WC, Su, Zartman, R.E., 2009. Porphyry copper-gold mineralization at Yulong, China, promoted by decreasing redox potential during magnetite alteration. Econ. Geol. 104 (4), 587–596.

Ni, P., Wang, G.G., Yu, W., Chen, H., Jiang, L.L., Wang, B.H., Zhu, H.D., Xu, Y.F., 2015. Evidence of fluid inclusions for two stages of fluid boiling in the formation of the giant Shapinggou porphyry Mo deposit, Dabie Orogen, Central China. Ore Geol. Rev. 65, 1078–1094.

Rasmussen, K.L., Mortensen, J.K., 2013. Magmatic petrogenesis and the evolution of (F:Cl:OH) fluid composition in barren and tungsten skarn-associated plutons using apatite and biotite compositions: case studies from the northern Canadian Cordillera. Ore Geol. Rev. 50, 118–142.

Richards, J.P., 2003. Tectono-magmatic precursors for porphyry Cu-(Mo-Au) deposit formation. Econ. Geol. Bull. Soc. Econ. Geol. 98 (8), 1515–1533.

Roedder, E., 1971. Fluid inclusion studies on porphyry-type ore deposits at Binghan, Utah, Butte, Montana and Climax, Colorado. Econ. Geol. 66 (1), 98–120.

Rusk, B.G., Reed, M.H., Dilles, J.H., Klemm, L.M., Heinrich, C.A., 2004. Compositions of magmatic hydrothermal fluids determined by LA-ICP-MS of fluid inclusions from the porphyry copper-molybdenum deposit at Butte, MT. Chem. Geol. 210 (1–4), 173–199.

Sillitoe, R.H., 2010. Porphyry copper systems. Econ. Geol. 105 (1), 3–41.

Sobolev, A.V., 1996. Melt inclusions in minerals as a source of principle petrological information. Petrology 4 (3), 209–220.

Sobolev, A.V., Danyushevsky, L.V., 1994. Petrology and geochemistry of boninites from the north termination of the Tonga Trench: constraints on the generation conditions of primary high-Ca boninite magmas. J. Petrol. 35 (5), 1183–1211.

Thomas, R., Webster, J.D., Heinrich, W., 2000. Melt inclusions in pegmatite quartz: complete miscibility between silicate melts and hydrous fluids at low pressure. Contrib. Mineral. Petrol. 139 (4), 394–401.

Tu, G.Z., 1989. On the alkali-rich intrusive rocks. Miner. Resour. Geol. 13 (3), 1–4 (in Chinese).

Turner, S., Arnaud, N., Liu, J., Rogers, N., Hawkesworth, C., Harris, N., Kelley, S., Van Calsteren, P., Deng, W., 1996. Post-collision, shoshonitic volcanism on the Tibetan Plateau: implications for convective thinning of the lithosphere and the source of ocean island basalts. J. Petrol. 37 (1), 45–71.

Ulrich, T., Gunther, D., Heinrich, C.A., 1999. Gold concentrations of magmatic brines and the metal budget of porphyry copper deposits. Nature 399 (6737), 676–679.

Wang, J.H., Yin, A., Harrison, T.M., Grove, M., Zhang, Y.Q., Xie, G.H., 2001. A tectonic model for Cenozoic igneous activities in the eastern Indo–Asian collision zone. Earth Planet. Sci. Lett. 188 (1), 123–133.

Wang, D.H., Qu, W.J., Li, Z.W., Ying, H.L., Chen, Y.C., 2004. Mineralization of porphyry copper molybdenum deposit in Honghe metallogenic belt of Jinshajiang - the concentration period: Re-Os isotope dating. Sci. China Ser. D Earth Sci. 34 (4), 345–349 (in Chinese).

Wang, G.G., Ni, P., Zhao, K.D., Wang, X.L., Liu, J.Q., Jiang, S.Y., Chen, H., 2012. Petrogenesis of the Middle Jurassic Yinshan volcanic-intrusive complex, SE China: implications for tectonic evolution and Cu–Au mineralization. Lithos 150, 135–154.

Wang, G.G., Ni, P., Zhao, C., Chen, H., Yuan, H.X., Cai, Y.T., Li, L., Zhu, A.D., 2015. A combined fluid inclusion and isotopic geochemistry study of the Zhilingtou Mo deposit, South China: implications for ore genesis and metallogenic setting. Ore Geol. Rev. 67, 109–126.

Wilkinson, J.J., Stoffell, B., Wilkinson, C.C., Jeffries, T.E., Appold, M.S., 2009. Anomalously metal-rich fluids form hydrothermal ore deposits. Science 323 (5915), 764–767.

Xie, Y.L., Hou, Z.Q., Xu, J.H., Yang, Z.M., Xu, W.Y., He, J.P., 2005. Evolution of multistage ore-forming fluid and mineralization: evidence form fluid inclusions in Yulong porphyry copper deposit, East Tibet. Acta Petrol. Sin. 21 (5), 1409–1415 (in Chinese).

Xu, L.L., 2011. The Diagenetic and Metallogenic Geochronology and Magmatic fO_2 Characteristics of Jinshajiang-Red River Porphyry Cu (Mo, Au) Metallogenic Systems (Ph D Dissertation of Graduate University of Chinese Academy of Sciences). pp. 1–181 (in Chinese).

Xu, X.W., Cai, X.P., Song, B.C., Zhang, B.L., Ying, H.L., Xiao, Q.B., Wang, J., 2006. Petrologic, chronological and geochemistry characteristics and formation mechanism of alkaline porphyries in the Beiya gold district, western Yunnan. Acta Petrol. Sin. 22 (3), 31–642 (in Chinese).

Xu, L.L., Bi, X.W., Hu, R.Z., Zhang, X.C., Su, W.C., Qu, W.J., Hu, Z.C., Tang, Y.Y., 2012. Relationships between porphyry Cu–Mo mineralization in the Jinshajiang–Red River metallogenic belt and tectonic activity: constraints from zircon U–Pb and molybdenite Re–Os geochronology. Ore Geol. Rev. 48, 460–473.

Zhang, Y.Q., Xie, Y.W., 1997. The geochronology and Nd, Sr isotopic characteristics of the Ailaoshan-Jinshajiang alkali-rich intrusive belt. Sci. China Ser. D Earth Sci. 27 (4), 289–293 (in Chinese).

Zhang, Y.Q., Xie, Y.W., Tu, G.Z., 1987. A preliminary study of the Ailao Shan Jinsha River alkali rich intrusive rocks and their relationship with the rift structure. Acta Petrol. Sin. 3 (1), 17–25 (in Chinese).

Zhao, Z.H., Xiong, X.L., Wang, Q., Bao, Z.W., Zhang, Y.Q., Xie, Y.W., Ren, S.K., 2002. Alkaline igneous rocks and related mineralization of large and super large copper gold deposit in China. Sci. China Ser. D Earth Sci. 3, 1–10 (in Chinese).